ABSTRACT

PARTICLE RESPONSE FUNCTION IN SAMARIUM AND EUROPIUM ISOTOPES

By

James Edward Duffy

The reactions $(\alpha,t)$ and $(\alpha,{}^{3}He)$ have been performed with 100-MeV $\alpha$-particles on targets of $^{144,148,152,154}Sm$ to investigate high lying proton strength distribution in $^{145,149,153,155}Eu$ and neutron strength distribution in $^{145,149,153,155}Sm$, respectively. The emitted particles were identified in the S-320 spectrograph using two $\Delta E$ gas counters and an E plastic scintillator. Some differences were observed in the spectra depending on the nuclear deformation. Strong transitions to high-lying proton and neutron states up to about 15 MeV excitation energy were observed. Angular distributions were measured from 2° to 25° for both $(\alpha,t)$ and $(\alpha,{}^{3}He)$ reactions. The extreme forward angle data points were necessary to determine the $\ell$-transfers. A smooth background, calculated using the $\alpha$-breakup model, was subtracted from the spectra for

excitation energies above 3 MeV. The background-subtracted spectra were divided into 520-keV wide bins and the angular distribution for each bin was fitted with DWBA calculations to obtain a strength distribution for each ℓ-value. The excitation energies, angular distributions, and strengths of the high-lying transitions suggest that they arise from proton and neutron stripping to high-spin outer subshells, e.g. $1h_{9/2}$ and $1i_{13/2}$ in $^{145,149,153,155}$Eu and $1h_{9/2}$, $1i_{13/2}$ and $1j_{15/2}$ in $^{145,149,153,155}$Sm. The deduced proton and neutron strength distributions are compared with predictions from the quasiparticle-phonon model and the interacting boson-fermion approximation model.

# PARTICLE RESPONSE FUNCTION IN SAMARIUM AND EUROPIUM ISOTOPES

By

James Edward Duffy

A DISSERTATION

Submitted to
Michigan State University
in partial fulfillment of the requirements
for the degree of

DOCTOR OF PHILOSOPHY

Department of Physics and Astronomy

1986

To my wife

Andrea Rose Micallef

ACKNOWLEDGMENTS

I would like to thank my advisor Gary Crawley for his guidance and direction. His constant support and inspiration provided the insight necessary to complete this Thesis.

I would also like to thank Raman Anantaraman for his charitable time and friendship.

There are several people to whom I owe acknowledgement: for serving on my committee, Aaron Galonsky and Alex Brown; for their recomendations regrding to this thesis topic, Sydney Gales, Patricia Massolo, V.G. Soloviev, Olaf Scholten and George Bertsch; members of the computer group, Barbara Pollack, Ron Fox, Skip Vandermolen, Lori Fedewa and Richard Au; for members of the mechanical design group, Mike Fowler, Al Gavalya and Craig Snow; Gary Westfall, who provided emotional support; and those individuals who participated and volunteered long hours to assist in my experiments, Hans van der Plicht, Bob Tickle, John Winfield, Joe Finck and Silvana Angius; and to the dedicated staff, students and faculty of the NSCL.

With any project one endeavors, there are those individuals whose professional affiliation evolves into a social association. Special thanks for the many times

shared with racketball buddies Don Lawton and Jack Ottarson. Through Pacman and prelims, marrage and moving, for countless fond memories I thank Mark, Mary, Mike and Pat Curtin. Many thanks to Virginia Crawford, Ellen Prost and Tom Warren. Lastly, much love and appreciation to my parents James and Rosemary Duffy, my wife's parents Vincent and Claudette Micallef and my loving wife Andrea Micallef.

TABLE OF CONTENTS

# LIST OF TABLES

LIST OF FIGURES

# CHAPTER I

## INTRODUCTION

The study of elementary modes of excitation, particularly in many-body systems, is of great interest in several areas of physics. In nuclear physics, there are numerous examples of such simple structures, including isobaric analogue states, giant resonances and single-particle and single-hole states. The concept of single-particle motion in the mean field of the nucleus is perhaps the most fundamental idea in nuclear structure physics and is the basis for the highly successful nuclear shell model.

Experimentally, single-nucleon transfer reactions [Au70] have been the probes most extensively used to study the properties of single-particle and single-hole states. These reactions are of two types: stripping and pickup. In stripping, a nucleon is transferred from the projectile to an unoccupied single-particle state in the target, thereby probing the distribution of particle strength in the final nucleus. In pickup, a nucleon is transferred to the projectile from an occupied state in the target, thereby

probing the distribution of hole strength in the final nucleus.

Since the early 1960's, many single-nucleon transfer reaction studies have been performed on nuclei throughout the periodic table, with low energy light-ion projectiles (p, d, t, $^3$He, $^4$He), to examine low excitation energies (less than 5 MeV) of the nucleus. Only recently, with the help of higher energy beams, have such studies been extended to explore single-particle and single-hole strength at higher excitation energies. This Thesis describes the investigation of single-particle states at high excitation energies (up to 15 MeV) in a set of samarium isotopes whose shapes range from spherical to deformed, using the ($\alpha$,t) and ($\alpha$,$^3$He) reactions. The $\alpha$-particle beam was chosen because it provides the lightest projectile with which both proton and neutron stripping can be studied using the methods of charged-particle spectroscopy.

In this Chapter, the techniques that have been developed over the years to investigate particle and hole states by means of single-nucleon transfer reactions will first be presented. Next, brief reviews of the results of pickup and stripping reactions on medium-heavy targets will be given, including the use of nuclear structure models to understand the results. Finally, the goals of this Thesis -- the investigation of particle states in the samarium isotopes -- will be discussed.

In reality, nuclear states are seldom true single-particle states. Most commonly, as sketched in Figure I.1, a given single-particle (or single-hole) excitation spreads over many states of the final nucleus. Transfer reactions then study the distribution of the single-particle strength over a finite energy interval. Such mixing of simple states with more complicated underlying states is a problem even at low excitation energies, and it becomes worse with increasing excitation.

In a single-nucleon transfer reaction, each state in the final nucleus is populated with a strength proportional to the square of the amplitude of the single-particle component of that state. This strength is usually expressed in terms of the spectroscopic factor S for that state. The precise mathematical definition of S will be given in Chapter III, in equation (III.13). Qualitatively, the spectroscopic factor $S_{n\ell j}$ for a state $|J_B,M_B\rangle$ in the residual nucleus B, of angular momentum $J_B$, is the probability that $|J_B,M_B\rangle$ "looks like" the target ground state $|J_A,M_A\rangle$ plus a particle p (or hole) in the single particle state $|n\ell j\rangle$. Here B=A+p. The angular momenta satisfy the relation $\vec{J}_B = \vec{J}_A + \vec{j}$.

The technique used to extract the spectroscopic factor S of a state is the following. From spectra taken at various angles, the experimental angular distribution for

Figure I.1

Fragmentation of a single-particle excitation.

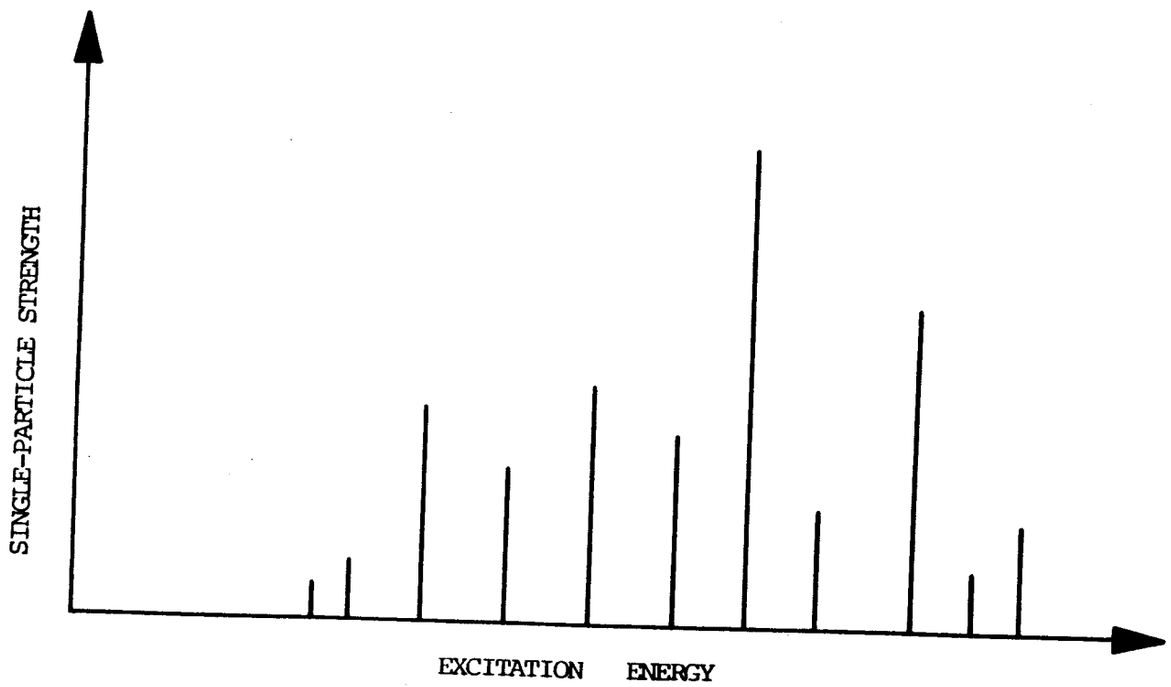


Figure I.1

the state is obtained. It is characteristic of the orbital angular momentum (ℓ) of the transferred particle; the j must be inferred from other considerations, such as the use of polarized beams. This angular distribution is compared with a theoretical one calculated in the Distorted Wave Born Approximation (DWBA) in which it is assumed that the entire spectroscopic strength is concentrated in that one state. The ratio of the experimental to the theoretical angular distribution then gives the actual S for that state. By studying different states, the distribution of S is mapped out. At higher excitation energies the level density becomes so large that individual states cannot be resolved in the transfer reactions. It is still possible to study the single-particle (and single-hole) excitations by the envelope of the strength distribution, which appears as a broad bump in a low resolution experiment. The details of this procedure and its uncertainties are discussed in Chapters III and IV.

This distribution of S as a function of excitation energy in the final nucleus contains a lot of nuclear structure information. The centroid of the distribution, for all fragments $|J_B, M_B\rangle$ of a given single-particle (or single-hole) excitation $|n\ell j\rangle$, gives the energy of that excitation. The width of the distribution is a measure of the spreading of the single-particle (or single-hole) excitation. The sum of the spectroscopic factors of all fragments of a given single-particle (or single-hole)

excitation measures the extent to which that excitation is empty (or occupied) in the target ground state.

The total width of a nuclear state is the sum of two parts: the decay width and the spreading width. The decay width or escape width of a state is a measure of the probability that the state decays to a lower energy state either in the same nucleus (by $\gamma$ emission) or in another nucleus (by particle emission). The spreading width is the probability that the state decays through the development of more complex excitations such as vibrational states, compound nuclear states, etc. In this mixing, the angular momentum of the initial single-particle is preserved: a state of angular momentum j mixes only with background states having the same total angular momentum.

When the lifetime of a state is known, its decay width can be easily calculated using the uncertainty principle. This is given by the following.

$$\Gamma = \frac{\bar{h}}{t} = \frac{\bar{h}c}{ct} = \frac{197\ (\text{MeV}\ \text{fm})}{3\times 10^{23}(\text{fm/sec})\times t(\text{sec})} \qquad (I.1)$$

Here t is the mean lifetime in seconds, which is related to the half life by the expression $t = 1.44 t_{1/2}$.

In this Thesis, we shall concentrate on the spreading width of the single-particle excitation, which is measured by the width of the distribution of all the complex states (shown in Figure I.1) into which the excitation fragments.

Each of these complex states has a width which arises from its decay to lower-lying states (the decay width). When the state is bound with respect to particle emission so that it decays only by γ-ray emission, it has a negligible decay width. For example, the first excited state of $^{145}$Sm has a half life of $36 \times 10^{-12}$ seconds [Tu80] and decays by γ-ray emission to the ground state with an energy of 0.883 MeV. Its decay width, calculated using equation (I.1), is $1.3 \times 10^{-8}$ keV. When the state is unbound with respect to particle emission, the decay width is much larger. It depends on the energy available for the decay, on the angular momentum in the decay channel, and on whether the decay is by proton or neutron emission, and can be estimated by performing a potential barrier penetration calculation. Normally, the decay is by neutron emission, since the Coulomb barrier inhibits charged particle emission. A typical value [Be86] for the single-particle decay width ($\Gamma_{s.p.}$) is 1 MeV when the decay energy is a few MeV. The decay width for any of the individual complex states will be reduced from this value depending on its spectroscopic factor, and may typically be 0.1 MeV for an unbound state. The spreading width for the single-particle excitation, on the other hand, is typically several MeV. Thus, for the situation of interest to us, the decay width can be ignored in comparison with the spreading width.

Many light ions at different incident energies have been used in pickup reactions, such as (p,d) and ($^{3}$He,α), to

investigate single-hole strength in medium - heavy nuclei [G1-1]. The beam energies have ranged from about 22 MeV for deuterons [Co69] to 283 MeV for $^{3}$He [La82]. Some of the studies have involved polarized proton beams and the use of the $\vec{(p,d)}$ reaction [Cr80]. Deep-lying neutron-hole states, i.e. neutron orbits deeply bound below the Fermi surface, in different isotopes of Zr, Sn, Sm and Pb have been studied by means of the (p,d) reaction at 42 MeV [Ga81] and the ($^{3}$He,$\alpha$) reaction at 70 MeV [Ga83]. These studies probed neutron-hole strength in the excitation energy range from about 4 to 15 MeV. Also the $^{90}$Zr$(\vec{p},d)^{89}$Zr reaction [Cr80] was used to extract the j-values of deep hole states using analyzing power measurements.

In all these cases, an underlying background was found in the spectra. In most cases, the background was drawn by hand to connect low points in the spectra. This rather arbitrary method led to uncertainties in the experimental cross sections, which were usually obtained by assuming specific peak shapes for gross structures. A series of different gaussian shapes spanned the entire energy region of the background-subtracted spectra and experimental cross sections were calculated using these gaussian shapes. Experimental angular distributions were plotted and compared with the theoretical angular distributions to yield the amount of strength for an individual $\ell$-transfer in that

energy region. The strengths of various ℓ-transfers were then calculated for the complete energy spectrum.

This gave the spreading of strength of deep hole states in medium and heavy nuclei over the excitation energy range investigated experimentally. Attempts were then made to understand the reasons for this spreading, by comparing the observed strength distribution with theoretical models. Such comparisons show that, at low excitation energies, the only important source of the spreading of single-hole states is the coupling to surface vibrations; the single-hole (and single-particle) mode decays by exciting these vibrations [Be79,So80,Be83a,Be83b,Sc85]. At higher excitation energies, the nucleons in the interior of the nucleus absorb energy more effectively from the simple modes. A model commonly used to treat this behavior is the quasi-particle phonon model [So80], which considers mixing with both low-lying and high-lying phonon states.

The hole state results for the samarium isotopes with neutron number larger than N=82 show a picture that is different from the one seen in the Cd, Pd, Sn and Te isotopes [Ga81,Sc80,We77,Ge80,Ga82a]. They show that the disappearance of the N=82 shell gap, as the deformation increases, leads to overlapping of the $h_{11/2}^{-1}$ hole strength with the strengths corresponding to the lower subshells, $2d_{5/2}^{-1}$ and $1g_{9/2}^{-1}$.

Since background subtraction in hole state analysis is a difficult problem, the more complicated particle-gamma

coincidence reaction ($^{3}$He,$\alpha\gamma$) was carried out on targets of $^{102,106,108}$Pd and $^{112,118}$Sn using a 70-MeV beam of $^{3}$He particles [Sa81,Sa85]. Here it was found that a large fraction of the $g_{9/2}^{-1}$ hole state strength in $^{101}$Pd occurred as a single state at $E_x$= 2.396 MeV with a width of 2.5 keV. The remaining $g_{9/2}^{-1}$ strength occurred in a 1-MeV wide bump at about 4 MeV excitation energy, which decayed statistically.

The information obtained from the extensive measurements of deep-lying hole states in nuclei is useful both because it helps in the development of models of nuclear structure and because the empirical values of the position and the width of particular hole states can be used as input for predictions of other nuclear phenomena such as giant resonances. Giant resonances are simple, usually collective excitations in nuclei which are excited in inelastic scattering processes as a superposition of particle - hole states [Be79]. In order to calculate their position and spreading width, information on the individual hole and particle states is useful [Be83a].

We next turn to measurements of the particle strength. This provides valuable information which is complementary to that on the hole strength. While it is possible to obtain information on hole states from knockout reactions like (p,2p), there are no analogous reactions to populate particle states. Such states are generally studied by stripping reactions. (If the state is unbound, it can also be studied by the direct scattering of nucleons, but this

technique is useful only over a limited range of excitation energies.) Unlike the situation with deep-hole states, until recently there has been little or no comparable information on highly excited particle states in medium and heavy nuclei [G1-2]. Understanding the potential of stripping reactions to provide information on high-lying particle states is an additional important motivation of this work.

Studies of particle states in spherical nuclei were recently carried out at Orsay [Ga82b,Ga83,Ga85a,b]. The stripping reactions used were $^{90}$Zr, $^{120}$Sn, $^{144}$Sm, $^{208}$Pb($^{3}$He,d) and $^{120}$Sn, $^{144}$Sm, $^{208}$Pb($\alpha$,t) for proton particle states and $^{90}$Zr, $^{120}$Sn, $^{208}$Pb($\alpha$,$^{3}$He) for neutron particle states. A 240 MeV beam of $^{3}$He particles and 80 MeV and 183 MeV beams of $\alpha$ particles were used to investigate particle state strength from about 4 to 15 MeV of excitation energy. The techniques used were essentially similar to those used to analyze the hole state strength [Ga81,Ga82a], but with some differences.

Two of the differences were the use of a plane wave breakup calculation to predict the underlying background and of a "slicing" method instead of the gaussians to extract the cross sections. The plane wave breakup calculation reproduced the spectral cross section at high excitation energy for the 240 MeV $^{3}$He and 183 MeV $\alpha$ particle beam cases but failed to do so for the 80 MeV $\alpha$ induced reactions. This was later found to be due to the fact that the 80 MeV $\alpha$

beam energy is too low for the plane-wave approximation to be valid, and so an empirical solution was developed using the shape of the breakup calculation.

Experimental cross sections were deduced using gaussian shaped peaks for the case of the 240 MeV $^{3}$He beam and using both gaussian shaped peaks and "slicing" the corrected spectra into bins for the 80 MeV and 183 MeV $\alpha$ particle beams. Experimental angular distributions were obtained using both the gaussian shapes and the "sliced" bins. Comparisons of the experimental and theoretical (DWBA) angular distributions yielded the amount of strength which each individual $\ell$-transfer had in a particular energy region. The strengths of various $\ell$-transfers were obtained for the complete energy spectrum measured.

The strength distributions were compared with theoretical models, in particular the quasi-particle phonon model [So80,St83]. These comparisons suggested that the spreading of states is due to surface vibrations interacting with the particle states in spherical nuclei, similar to the mechanism for the hole states.

The present work is an extension of such particle-strength studies to deformed nuclei, for which no information on high-lying particle strength has been available until now. Since the spreading of the states is predicted to depend on the phonon structure of the nucleus, studies of deformed nuclei, in which the phonon structure is quite different from that in spherical nuclei, provide a

useful test of the theory. In addition, this will also provide us with a complete set of both proton and neutron particle states for an isotope chain that changes its phonon structure. We elected to use the even-even samarium isotopes as targets because they range from spherical, as in the $^{144}$Sm case, to very deformed, as in $^{154}$Sm. The deformation of the samarium isotopes, estimated from the variation of the B(E2) values of the first $2^+$ state in these nuclei, ranges from $\beta_2$=0.0 for $^{144}$Sm to $\beta_2$=0.27 for $^{154}$Sm [Go72].

The goal of this investigation is to obtain information on the single particle strength distribution as a function of the deformation of the target nucleus. The overlapping of high lying proton strength distributions will be compared with the lower energy work mentioned above, for the spherical nucleus $^{144}$Sm. Finally, comparisons of data to theory, will be carried out where possible.

This Thesis is divided into six chapters and two appendices. Chapter II: The experimental procedure that was used to obtain the stripping data is discussed. With a beam of 100-MeV $\alpha$ particles, the stripping reactions $(\alpha,t)$ and $(\alpha,^3He)$ were used to investigate the proton and neutron particle states, respectively, in the isotopes of samarium. Targets of $^{144,148,152,154}$Sm were used. The $\alpha$-particle

energy (100 MeV) was selected to be high enough to excite high ℓ-transfers.

Chapter III: A presentation of the DWBA theory is given in this chapter.

Chapter IV: This chapter explains the technique used to extract spectroscopic information from the stripping reaction data. First, a background is calculated and subtracted from the spectra. The background is taken to consist of two parts: a breakup part, calculated in the plane wave model, and a compound nuclear emission part. Next, a "slicing" technique is used on the background-subtracted spectra to extract the experimental cross sections.

Chapter V: Experimental angular distributions are plotted and compared with the theoretical DWBA calculations to yield the strength. The results obtained using this technique are presented.

Chapter VI: The experimental results are compared with the theoretical calculations that exist for five of the eight final nuclei studied here. The conclusions of this investigation are also presented.

Appendix I: This appendix lists the $(\alpha,t)$ and $(\alpha,{}^{3}He)$ cross sections as a function of angle for the low lying states populated in the reactions on

$^{144}$Sm and $^{208}$Pb, the low lying peaks populated in the reactions on $^{148,152,154}$Sm and the elastic scattering cross sections for $^{144,148,152,154}$Sm($\alpha,\alpha$).

Appendix II: This appendix outlines, in an algorithm style format, two of the main programs developed for this Thesis: the calibration program SPECCAL and the analysis program SMASHER. Sample input files to run these and other programs used in this Thesis are also given.

## CHAPTER II

## EXPERIMENTAL PROCEDURE

The measurements of $(\alpha,t)$ and $(\alpha,{}^3He)$ reactions described in this Thesis were carried out using an $\alpha$-particle beam from the K500 cyclotron at the National Superconducting Cyclotron, Michigan State University. The experiment required three runs which spanned about one and a half years. During this time many improvements in the data taking system were developed. Specific changes in the detector equipment and the data acquisition system will be referred to throughout this Chapter.

### II.1 EXPERIMENTAL SETUP

The beam energy used was 100 MeV, with beam intensities on target ranging from 25 to 200 particle nanoamperes. The targets used were 0.88 mg/cm$^2$ Mylar $(C_{10}H_8O_4)_n$, 1.0 mg/cm$^2$ $^{144}$Sm (96.47% isotopic enrichment), 3.0 mg/cm$^2$ $^{148}$Sm (90.70%), 4.7 mg/cm$^2$ $^{152}$Sm (98.29%), 3.9 mg/cm$^2$ $^{154}$Sm (98.69%) and 6.0 mg/cm$^2$ $^{208}$Pb. The samarium targets were purchased from the company Micromatter, Inc. of Seattle, Washington. Elastic cross sections were used to obtain the

thicknesses of the Sm targets. The elastic cross section measurements were carried out at lab angles of 2°, 4° and 6° using the 100 MeV α-beam. The calculated elastic to Rutherford scattering cross section ratio using the code DWUCK4 [Ku69] has values of 1.01, 1.02 and 1.14, respectively, at lab angles of 2°, 4° and 6° for $^{144}$Sm and similar values for the other three targets. The target thicknesses were determined by matching the calculated to the measured cross sections. Uncertainties in the target thickness for the samarium isotopes $^{144,148,152,154}$Sm are respectively 7%, 7%, 20% and 6%. The measurement for $^{152}$Sm has the largest uncertainty because the cross section at one of the angles (4°) was about 20% above the fitted theoretical angular distribution curve, making the normalization uncertain.

The stripping cross section measurements were carried out at lab angles from 2° to 25°, generally in 1° to 2° steps at the forward angles (below 9°) and in 3° steps at the backward angles (above 11°). The energy resolution of our experiment was limited by the S320 spectrograph system and not by the target thicknesses. The resolution was tested using the elastic peak in the focal plane of the S320 spectrograph. Adjustments of the x-quadrupole, sextupole and octupole magnets, the gas pressure in the focal plane detector, and the electronic gains were carried out with the elastic peak at various positions in the focal plane of the spectrograph, to achieve the best resolution possible. This

was found to be 280 keV at small angles and up to 320 keV at the larger angles for the (α,t) reactions. A somewhat better resolution (≈200keV) was found for the (α,$^3$He) reactions, probably because the extrapolation of the spectrometer parameters from the elastic scattering settings was smaller in this case than in the (α,t) case.

The tritons and $^3$He particles were detected in the focal plane of the S320 spectrograph. A view of this spectrograph is given in Figure II.1 [Be83b]. The S320 system consists of a scattering chamber, the five magnets of the spectrograph (two quadrupoles, a dipole, an octupole, and a sextupole) and a focal plane detector. One quadrupole focuses in the y-direction and the other in the x-direction. The dipole magnet enables one to measure the magnetic rigidity (p/q) of the emitted particles, where p is the linear momentum and q the charge of the emitted particle. The octupole and sextupole magnets are used to focus the particles at the focal plane of the detector and to compensate for higher order aberrations.

The detector consists of two position sensitive wire chambers (one in the front part and one in the middle part of the detector), two ion chambers (one in the front and one in the back part), a grid and a 3-inch thick piece of plastic scintillator located at the end of the detector. A diagram of the detector box is displayed in Figure II.2 [Sh85].

Figure II.1

View of the NSCL S320 spectrograph [Be83b].

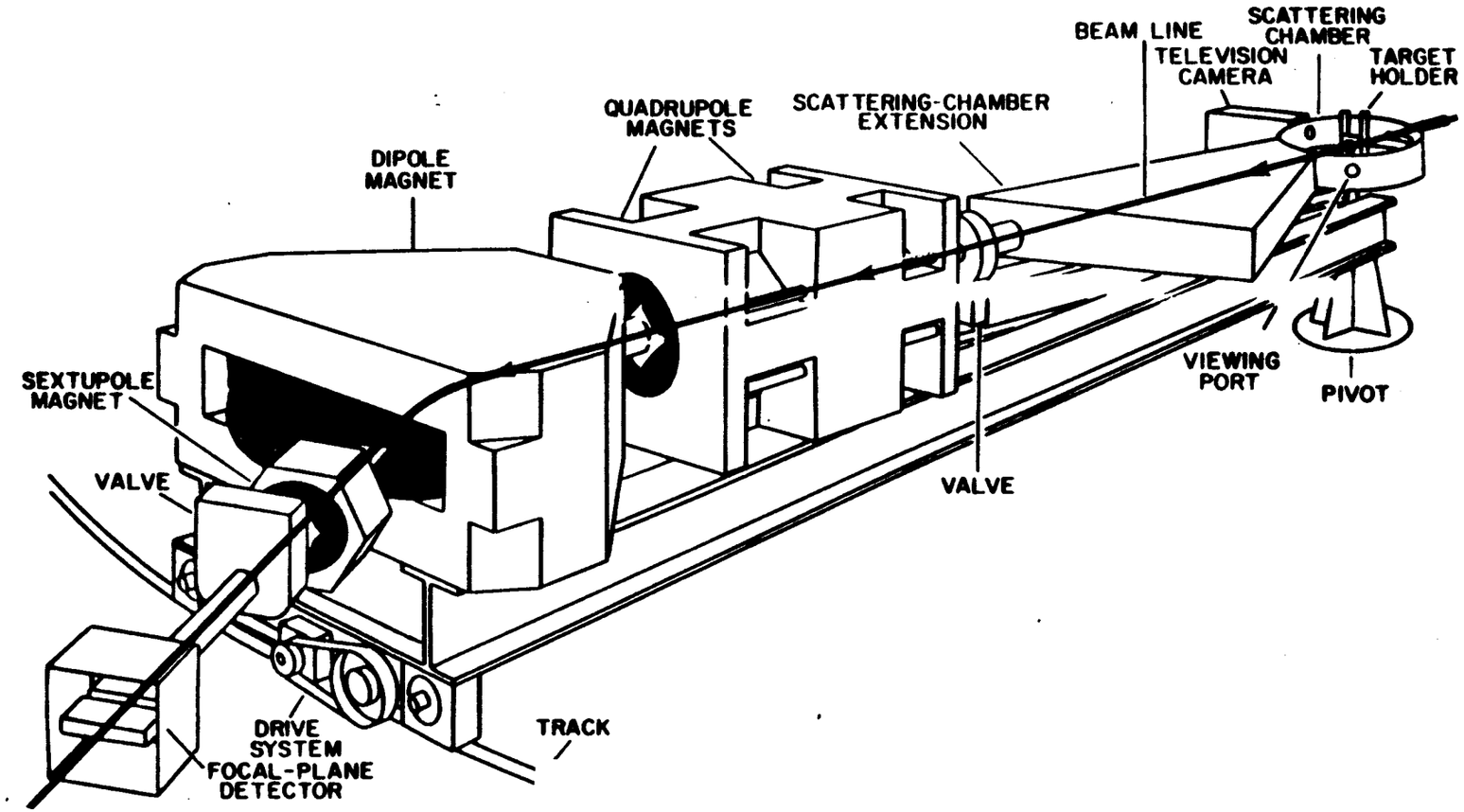
BEAM LINE
SCATTERING CHAMBER
TELEVISION CAMERA
TARGET HOLDER
QUADRUPOLE MAGNETS
SCATTERING-CHAMBER EXTENSION
DIPOLE MAGNET
SEXTUPOLE MAGNET
VALVE
VIEWING PORT
PIVOT
VALVE
DRIVE SYSTEM
FOCAL-PLANE DETECTOR
TRACK

Figure II.1

Figure II.2

View of the NSCL S320 detector box.

FWPC => Front wire proportional counter.

FIC => Front ion chamber.

BIC => Back ion chamber.

BWPC => Back wire proportional counter.

SC => Scintillator.

PM => Photo multiplier tube.

MSU-84-627

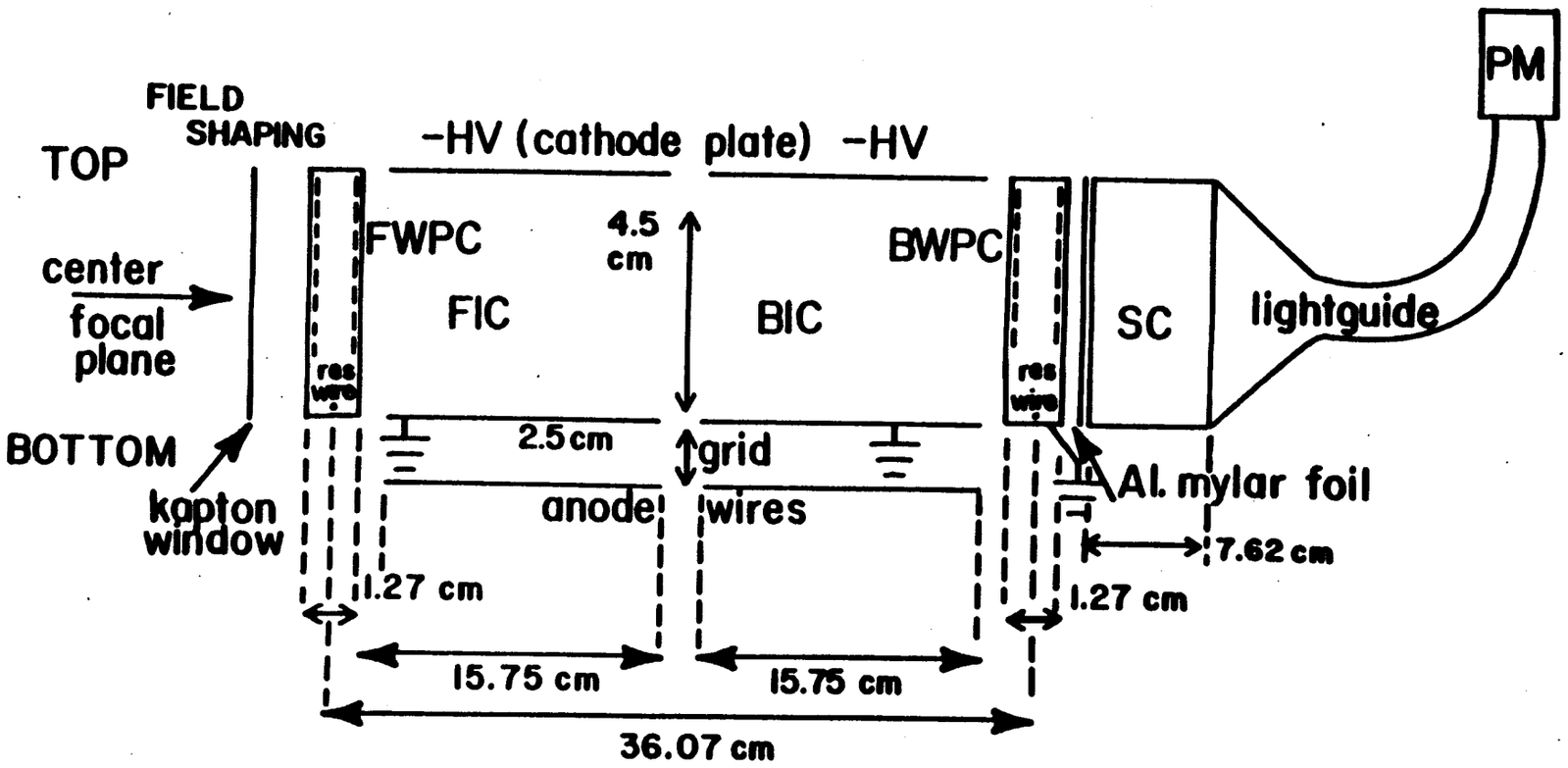


Figure II.2

Typical settings of the spectrograph magnets used for the (α,t) and (α,$^3$He) reactions of interest are given in Table II.1, in terms of both potentiometer and digital voltmeter (DVM) readings. These settings were used to focus the highest energy tritons or $^3$He onto the focal plane of the S320, which is at the position of the front position sensitive wire chamber. The highest energy particles emitted were focused near one end of the focal plane because this enabled the examination of the excitation energy range from 0 to 15 MeV. The settings were obtained from a program called S320 [Va85a]. A more detailed description of the S320 spectrograph is given in another NSCL Thesis [Sh85].

Two collimators of different sizes, one narrow and one wide, were used during the experiment. The narrow one was used to decrease the count rate at the forward angle of 2° and the wide one was used for the other angles. The narrow collimator was made of copper, with a thickness of 0.125 inches (enough to stop 90 MeV $^3$He) and an aperture of 1.0 by 2.0 inches. The wide collimator, which was the most frequently used one, was made of brass with a thickness of 0.25 inches (enough to stop 90 MeV tritons) and had an opening of 1.6 by 1.6 inches. Both were located 78.5 inches from the target ladder.

A number of different Faraday cups were used in the experiment. In the first two runs, two Faraday cups were

Table II.1

Typical S320 magnet settings for $^{148}Sm(\alpha,t)$ and $^{148}Sm(\alpha,^{3}He)$ reactions at $T_{\alpha}$= 100 MeV and $\theta_{lab}$= 6°.

| S320 | Reaction | | | | |
|---|---|---|---|---|---|
| Magnet | $^{148}Sm(\alpha,t)$ | | | $^{148}Sm(\alpha,^{3}He)$ | |
| | Pot | DVM | | Pot | DVM |
| $Q_{20}$ (Y) | 12.48 | 1.221 | V | 5.72 | 0.559 V |
| $Q_{21}$ (X) | 3.001 | -27.835 | V | 1.375 | -12.752 V |
| Dipole | 7.34 | 13.407 | kG | 3.25 | 6.142 kG |
| Octupl. | 297. | 12.638 | V | 136. | 5.790 V |
| Sext. | 390. | 15.508 | V | 179. | 7.105 V |

used for different angles of the spectrograph. One cup was located in the target chamber and was designed to measure charge for scattering angles of 12° and larger. This Faraday cup did not have an electron suppressor, thus posing a problem with normalization. The other cup was located in the wedge and had an electron suppressor. This cup was used to measure the charge for scattering angles from 2° to 9°. In the third run, we used a single Faraday cup with an electron suppressor. This was located in the target chamber and was designed to measure the charge for scattering angles of 4° and larger. It was called the zero degree Faraday cup. It did not fulfill all of our needs, due to its inability to allow the particles of interest to travel freely to the focal plane of the spectrograph for angles of 2° and 3°. To obtain spectra at 2° and 3°, we removed the zero degree Faraday cup and normalized using the wedge Faraday cup.

All of the measurements carried out for this Thesis were normalized using the zero degree Faraday cup. Short runs of spectra at the larger angles ($\geq$ 12°) for the ($\alpha$,t) reactions and at all angles for the ($\alpha$,$^3$He) reactions were taken using this Faraday cup, and these were used to normalize the spectra taken before the third run. Errors in this relative normalization are included in all the cross sections quoted in this Thesis.

Because of the problem in measuring the charge during the first run, a monitor detector was used to check the normalization in the second run. The monitor detector was used before the zero degree Faraday cup was installed and so was the only means available at the time to check the normalization. It was a simple device, consisting of a single piece of plastic scintillator, as displayed in Figure II.3. It had dimensions of 0.25 by 0.25 inches by 0.75 inches thick and was made of NE102. The light pulses from the NE102 were transferred through a fiber optic cable to a photomultiplier tube. The monitor was positioned at 18° in the plane of the beam and subtended a solid angle of about 0.4 msr. We chose the angle of 18° because the angular distribution of $\sigma_{el}/\sigma_{Ruth}$ for the elastic cross section on the Sm isotopes is predicted to be flat at 18°.

Typical spectra from the monitor are displayed in Figure II.4. Note the difference between the monitor spectra when the S320 spectrograph was at 7° and at 12°. When the S320 angle was 12° or larger, the monitor spectra showed some background. At the time, as mentioned before, there were two different Faraday cups to read the charge: a wedge Faraday cup and a target chamber Faraday cup. At an angle of 12°, the latter was only about an inch away from the monitor. The background in the monitor spectrum was presumed to be due to $\gamma$-rays and neutrons emitted from the

Figure II.3

A view of the monitor detector.

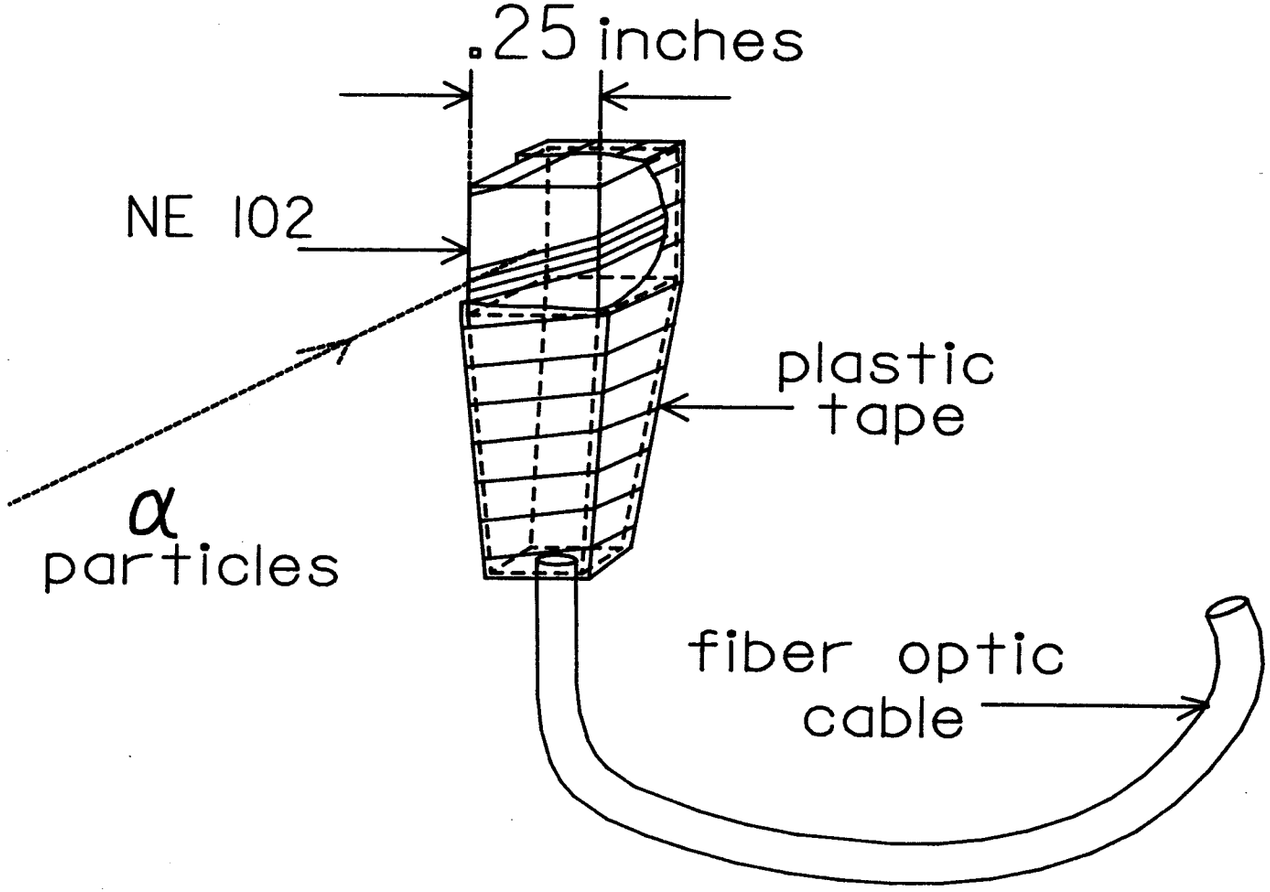


Figure II.3

Figure II.4

Typical spectra from the monitor detector. The $^{148}Sm(\alpha,^{3}He)$ monitor events with the S320 scattering angles at 7° and 12° are displayed on the left. The blank frame [empty$(\alpha,^{3}He)$] monitor events with the S320 scattering angles at 7° and 12° are displayed on the right.

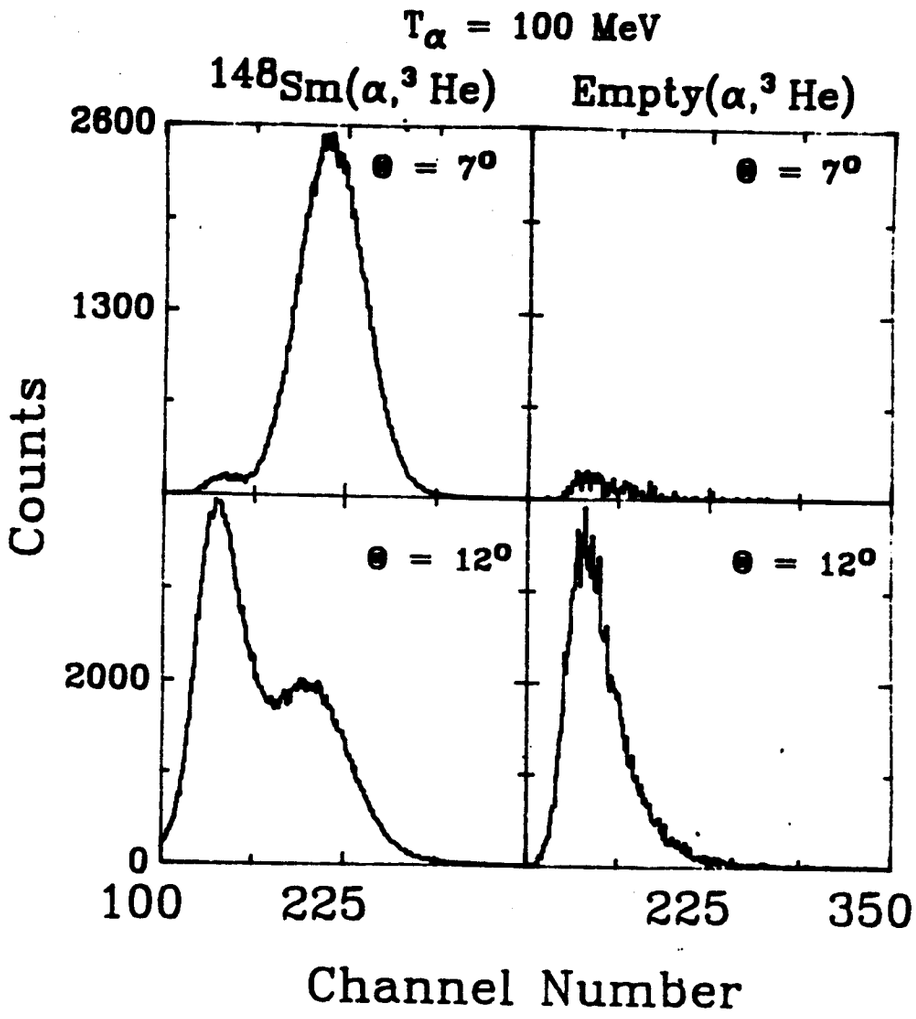
$T_\alpha$ = 100 MeV
$^{148}$Sm(α,$^3$He)
Empty(α,$^3$He)
θ = 7°
θ = 7°
θ = 12°
θ = 12°
2600
1300
2000
0
Counts
100
225
225
350
Channel Number

Figure II.4